


Therapeutic siRNA targeting *PLIN2* ameliorates steatosis, inflammation, and fibrosis in steatotic liver disease models

Yao Wang¹, Jiaxin Zhou¹, Qi Yang¹, Xinmeng Li², Yifu Qiu^{3,2}, Yansong Zhang^{1,4,*}, Min Liu^{1,3,*}, and Alan Jian Zhu^{1,3,4,*}

¹Ministry of Education Key Laboratory of Cell Proliferation and Differentiation, School of Life Sciences, ²Institute of Molecular Medicine, Beijing Key Laboratory of Cardiometabolic Molecular Medicine, College of Future Technology, and ³Peking-Tsinghua Center for Life Sciences, Academy for Advanced Interdisciplinary Studies, Peking University, Beijing, China; and the ⁴Peking University Chengdu Academy for Advanced Interdisciplinary Biotechnologies, Chengdu, Sichuan, China

Abstract Metabolic dysfunction–associated steatotic liver disease (MASLD) is the most prevalent chronic liver disease worldwide. If left untreated, MASLD can progress from simple hepatic steatosis to metabolic dysfunction–associated steatohepatitis, which is characterized by inflammation and fibrosis. Current treatment options for MASLD remain limited, leaving substantial unmet medical needs for innovative therapeutic approaches. Here, we show that *PLIN2*, a lipid droplet protein inhibiting hepatic lipolysis, serves as a promising therapeutic target for MASLD. Hepatic *PLIN2* levels were markedly elevated in multiple MASLD mouse models induced by diverse nutritional and genetic factors. The liver-specific deletion of *Plin2* exhibited significant anti-MASLD effects in these models. To translate this discovery into a therapeutic application, we developed a GalNAc-siRNA conjugate with enhanced stabilization chemistry and validated its potent and sustained efficacy in suppressing *Plin2* expression in mouse livers. This siRNA therapeutic, named GalNAc-si*Plin2*, was shown to be biosafe in mice. Treatment with GalNAc-si*Plin2* for 6–8 weeks led to a decrease in hepatic triglyceride levels by approximately 60% in high-fat diet- and obesity-induced MASLD mouse models, accompanied with increased hepatic secretion of VLDL-triglyceride and enhanced thermogenesis in brown adipose tissues. Eight-week treatment with GalNAc-si*Plin2* significantly improved hepatic steatosis, inflammation, and fibrosis in high-fat/high fructose-induced metabolic dysfunction–associated steatohepatitis models compared to control group. As a proof of concept, we developed a GalNAc-siRNA therapeutic targeting human *PLIN2*, which effectively suppressed hepatic *PLIN2* expression and ameliorated MASLD in humanized *PLIN2* knockin mice.  Together, our results highlight the potential of GalNAc-si*PLIN2* as a candidate MASLD therapeutic for clinical trials.

Supplementary key words fibrosis • GalNAc-siRNA • hepatic steatosis • inflammation • MASLD • *PLIN2*

Metabolic dysfunction–associated steatotic liver disease (MASLD) is the most common chronic liver condition, affecting over one-third of the global population (1). The disease spectrum of MASLD ranges from simple steatosis, characterized by hepatic lipid accumulation, to metabolic dysfunction–associated steatohepatitis (MASH), which includes inflammation and fibrosis (2, 3). Without intervention, MASLD can progress to cirrhosis, liver failure, or even cancer (4).

Despite substantial research efforts over the past decade (5, 6), MASLD treatment remains problematic. To date, only one drug therapy has been approved by the Food and Drug Administration (FDA) for MASLD (7). This limited progress can be attributed to the complex pathogenesis of MASLD, influenced by both genetic and environmental factors, posing significant challenges to drug efficacy (2). Consequently, current clinical management of MASLD primarily relies on lifestyle modifications such as calorie restriction and increased physical activity (8, 9). However, patients often find adherence to these lifestyle changes challenging, leading to suboptimal outcomes. Therefore, there is an urgent need for the development of well-tolerated, highly effective therapeutic interventions to address the unmet medical needs of MASLD patients.

Lipid droplet (LD) accumulation is a hallmark of the MASLD spectrum. Previous research has shown that LD clearance not only improves MASLD but also serves as a curative treatment for the disease (10, 11). *PLIN2*, a member of the PAT family proteins and a

*For correspondence: Alan Jian Zhu, zhua@pku.edu.cn; Min Liu, liumin02@pku.edu.cn; Yansong Zhang, zhangyansong@pku.edu.cn.

known master regulator of lipid homeostasis (12), is located on the surface of LDs and protects LDs from lipolysis by ATGL (13). Recent studies from our group and others have demonstrated a gradual upregulation of PLIN2 in MASLD mouse models and human MASLD patients (14, 15). Furthermore, genetic inhibition of PLIN2 has been shown to confer resistance to hepatic steatosis in mice (16–18), indicating a significant role of PLIN2 in the progression of MASLD. These findings also suggest that inhibiting PLIN2 may be sufficient to impede inflammation and fibrosis in MASH, the progressive form of MASLD.

Small-molecule inhibitors and siRNA therapy are two promising therapeutic modalities for targeting specific proteins. The screening for small-molecule inhibitors requires suitable binding pockets on target protein surfaces. However, the structural analysis of PLIN2 protein, performed using AlphaFold prediction, reveals a simplistic hydrophobic architecture devoid of binding pockets conducive to small-molecule interaction, characterizing it as undruggable to a significant extent (19). This, coupled with its functionality being primarily mediated by LD-targeting helices, facilitating its localization to the surface of LDs (13), rather than through enzymatic processes, poses considerable challenges for small molecule-based intervention. However, the approval of the first siRNA-based therapy by the FDA in 2018, along with the market introduction of four additional siRNA therapeutics (20, 21), highlights the potential of siRNA-based therapies as an alternative approach to modulate PLIN2 and address the therapeutic challenges in MASLD.

In this study, we have developed and chemically modified GalNAc-si $Plin2$ / $PLIN2$, an siRNA agent demonstrating satisfactory efficacy and high biosafety in multiple MASLD/MASH mouse models. Structurally, this agent comprises siRNA molecules chemically modified to prolong duration of action and ensure efficient delivery to the liver. GalNAc-si $Plin2$ efficiently suppressed $Plin2$ expression in hepatic tissues of mice without adverse effects. Importantly, our comprehensive evaluation revealed that this siRNA agent significantly ameliorated steatosis, liver injury, inflammation, and fibrosis across various preclinical models of MASLD/MASH. Mechanistically, our data suggest that GalNAc-si $Plin2$ promotes the secretion of VLDL triglyceride (TG), which serves as lipid fuel for the activated thermogenesis. Utilizing humanized $PLIN2$ knockin (KI) mouse models, we validated the efficacy of the human-targeted GalNAc-si $PLIN2$ formulation in suppressing $PLIN2$ expression and ameliorating MASH-associated pathology. These findings underscore the translational potential of GalNAc-si $PLIN2$ as a promising novel therapeutic candidate for addressing the complexities of MASLD management.

MATERIALS AND METHODS

Reagents

PowerUp™ SYBR™ Green Master Mix (Cat# A25776) and Lipofectamine™ 2000 Transfection Reagent (Cat# 11668019) were purchased from Thermo Fisher Scientific. Lomitapide (Cat# HY-14667) was purchased from MedChemExpress. D-Fructose (Cat# CF5421) was purchased from Coolaber. Tyloxapol (Cat# CF5421) was purchased from Macklin. Polyethylenimine (PEI, Cat# MW40000) was purchased from Yeasen Biotechnology. PLIN2 (mouse) antibody (Cat# Ab52356) and PLIN2 (human) antibody (Cat# Ab108323) were purchased from Abcam. F4/80 antibody (Cat# A23788), LC3B antibody (Cat# A7198), and MTP antibody (Cat# A1746) were purchased from Abclonal.

Mouse models

All animal housing and the experimental procedures were conducted in accordance with animal protocols approved by the Institutional Animal Care and Use Committee of Peking University, an AAALAC certified animal facility. Mice were housed in a controlled environment within the Peking University animal facility, with a 12 h light/dark cycle, a temperature of 22°C, and a humidity range of 40–60%. C57BL/6J mice were purchased from Charles River Laboratories International. *ob/ob* (JAX:000632) and Cre-dependent *spCas9* KI mice (JAX:026,556) (22) were obtained from the Jackson Laboratory. Humanized $PLIN2$ KI mice were generated by BIOCYTOGEN Company. Mice were provided with normal chow diet (10 kcal% of fat; Research Diets; Cat# D12450B) and access to water, except as specified. The MASLD model was established by feeding a high-fat diet (HFD, 60 kcal% of fat; research diets; Cat# D12492) to mice aged 6–8 weeks for a duration of 12 weeks. The MASH mouse models were developed by feeding a methionine/choline-deficient diet (21% fat; research diets; Cat# A02082002B) for 3 weeks, or HFD/high-fructose (HFr) diet (30% fructose water and HFD; research diets; Cat# D12492) for 16 weeks to mice aged 6–8 weeks. At the conclusion of the study, mice were anesthetized, sacrificed, and liver and blood samples were collected for histological and biochemical analysis.

Cell culture

HEK293T cells (Cat# R70507) were obtained from Thermo Fisher Scientific. HepG2 cells (Cat# HB-8065, RRID:CVCL_0027) were obtained from ATCC. AML12 cells (Cat# CTCC-400-0368) were acquired from MeisenCTCC. All cells were cultured in DMEM (Thermo Fisher Scientific; Cat# C11995500BT) supplemented with 10% FBS (CellMax; Cat# SA201.02) and 1% penicillin/streptomycin (P/S; Thermo Fisher Scientific; Cat# 15140122) at 37°C with 5% CO₂. During plasmid DNA transfection for adeno-associated virus (AAV) packaging, PEI (Yeasen Biotechnology; Cat# MW40000) was used according to the manufacturer's protocol. For siRNA transfection in mammalian cells, Lipofectamine™ 2000 Transfection Reagent (Thermo Fisher Scientific; Cat# 11668019) was used. Twelve hours post-transfection, cells were incubated in medium supplemented with 100 mM sodium oleate (Sigma-Aldrich; Cat# O7501) to increase the basal lipid content. Another 12 h or 36 h later, the cells were harvested for quantitative real-time PCR or immunoblotting, respectively.

Generation of AAV DNA vector

For CRISPR/Cas9-mediated acute gene knockout in the liver, a recombinant AAV DNA vector [pX602-AAV-Cre-small guide RNA (sgRNA)] was generated from the parental vector pX602-AAV-TBG::NLS-SaCas9-NLS-HA-OLLAS-bGHpA;U6::BsaIsgRNA (Addgene; Cat# 61593). pX602-AAV-Cre-sgRNA vector contains the liver-specific TBG promoter, Myc-tagged Cre recombinase for the recombination of loxP-flanked stop codon, and the human U6 promoter for non-coding sgRNA transcription. sgRNAs were designed using the E-CRISP platform (<http://www.e-crisp.org/>) according to the predicted specificity, annotation, efficacy) score to optimize editing efficiency while reducing the risk of off-target effects. A sgRNA targeting *LacZ* was included as a control. sgRNA sequences are listed in the [supplemental Table S1](#).

AAV production and delivery

AAV vectors were packaged and produced in HEK293T cells. In brief, when HEK293T cells reached approximately 80% confluence, they were cotransfected with AAV transfer plasmids (7 mg/15 cm dish), helper plasmids (20 mg/15 cm dish), and Rep/Cap(2/8) plasmids (7 mg/15 cm dish) using PEI. The culture media were changed 16 h after transfection, and the cells were harvested for AAV purification 60 h posttransfection. Viral purification and titer quantification were conducted using standard procedure (23). Specifically, the titer of the purified virus was determined by RT-qPCR. AAV delivery was performed via tail vein injection. For the knockout of hepatic *Plin2* gene in mouse liver by CRISPR/Cas9, *spCas9*KI mice (6–8 weeks old) were administered with AAV-Cre-sgRNA at 2×10^{11} viral genome copies and sacrificed after 6 weeks.

Generation and chemical modification of siRNAs targeting PLIN2/*Plin2*

To generate siRNAs targeting the conserved region of human *PLIN2* and mouse *Plin2* mRNA sequence, we designed siRNAs derived from human *PLIN2* and mouse *Plin2* CDS sequences on the DSIR platform (<http://biodev.extra.cea.fr/DSIR/DSIR.html>), respectively. Subsequently, two siRNAs targeting the same conserved region of *PLIN2/Plin2* of these two species with high scores were selected to serve as a pair of candidates. Finally, 5 pairs of siRNA candidates were selected, and the sequence information are listed in [supplemental Table S2](#). The production and chemical modifications of siRNAs were performed by Suzhou Biosyntech.

Subcutaneous injection of siRNA agent

The siRNA agent was diluted with PBS to achieve a final concentration at 7 A/ml solution. Following the induction of MASLD/MASH, the mice were randomly assigned to receive injections of PBS, GalNAc-siNC, or GalNAc-si*Plin2/PLIN2* (4 mg/kg) via syringe administration while under isoflurane anesthesia. The subcutaneous injection site was the dorsal side of the neck.

Quantitative real-time PCR

Total RNA was extracted from frozen tissue samples or cells by the Eastep Super Total RNA Extraction Kit (Promega; Cat# LSI040). First-strand cDNA was synthesized with the Eastep RT Master Mix Kit (Promega; Cat# LS2050). Real-time PCRs were performed on the Applied Biosystems 7,500 real time PCR system (Thermo Fisher Scientific) using PowerUp

SYBR Green Master Mix (Thermo Fisher Scientific; Cat# A25776). *Gapdh/GAPDH* or *Actb* were used as the reference gene. The primer sequences used are listed in [supplemental Table S3](#). To quantify the RT-PCR results, the relative fold changes in gene expression were calculated using the comparative Ct ($2^{-\Delta\Delta Ct}$) method, where values were normalized to a reference gene.

Immunoblotting

Frozen tissue or cell samples were first lysed in RIPA lysis buffer [50 mM Tris-HCl (Sigma-Aldrich; Cat# T1530), 150 mM NaCl, 0.1% SDS (JSENB; Cat# JS0054), 1% NP-40 (Sigma-Aldrich; Cat# I8896), 0.5% sodium deoxycholate (Sigma-Aldrich; Cat# D6750), pH 8.0] supplemented with EDTA-free protease inhibitor cocktail (Roche; Cat# 13538100). Subsequently, the lysates were separated by SDS-PAGE gel electrophoresis, and the proteins were transferred to PVDF membrane for immunoblotting. The membrane was then blocked for 1 h at room temperature in PBS plus 0.1% Tween-20 (PBST; Sigma-Aldrich; Cat# P1379) containing 5% skim milk. Following blocking, the membrane was incubated with primary antibodies in PBST containing 2.5% skim milk at 4°C overnight. After washing with PBST, the blot was incubated with secondary antibodies for 1 h at room temperature.

H&E staining, Oil red O staining, and TUNEL staining

For histology analysis, the liver and other organs were fixed in 4% paraformaldehyde (PFA; Sigma-Aldrich; Cat# 441244) for at least 24 h, followed by paraffin embedding. H&E staining and Oil red O staining was used to visualize the pattern of steatosis in the liver. For Oil red O staining, frozen liver tissues were prepared in OCT compound. Frozen tissues were then cryo-sectioned at a thickness of 15 μ m and stained with Oil red O (Beyotime; Cat# C1058M) according to manufacturer's protocol. The nuclei were stained by immersing the tissue slides in hematoxylin solution (Shanghai Yuanye; Cat# R20570) for 1 min. TUNEL staining was performed to evaluate liver injury, following the instructions provided with the TUNEL Apoptosis Assay Kit (Appligen; Cat# C0002).

Immunohistochemistry

Macrophage infiltration in hepatic tissues was detected using F4/80 immunohistochemistry. Antigen retrieval was first performed by subjecting the paraffin-embedded mouse liver sections to microwave treatment with EDTA antigen retrieval solution (Leagene; Cat# IH0304) for 1 h. The endogenous peroxidase activity was then quenched by incubating the sections in endogenous peroxidase blocking buffer (Beyotime; Cat# P0100B) for 10 min at 37°C. Subsequently, the sections were blocked with 5% BSA for 60 min at room temperature. Primary antibodies were used to detect the expression of the indicated proteins. After incubation with HRP-conjugated secondary antibodies, the sections were visualized using the DAB HRP color development kit (Beyotime; Cat# P0203) according to manufacturer's instructions. Finally, the slides were stained with hematoxylin (Shanghai Yuanye; Cat# R20570), dehydrated, and mounted for bright-field microscopy.

Immunofluorescence

For immunofluorescence staining, the frozen tissues were cryo-sectioned at a thickness of 15 μ m and fixed in 4% PFA

for 15 min. After fixation, the samples were permeabilized in PBS containing 0.1% Triton X-100 (Sigma-Aldrich; Cat# T8787) for 5 min. Samples were then incubated with primary antibody overnight at 4°C and washed with PBS three times. Samples were further incubated with secondary antibody for 2 h at room temperature and washed with PBS three times. After the final wash, the samples were incubated with 0.01 mg/ml 4',6-diamidino-2-phenylindole (Thermo Fisher Scientific; Cat# D1306) and 1 µg/ml BODIPY 493/503 (Invitrogen; Cat# D3922) for 5 min. Finally, the samples were mounted and used for image acquisition with a Leica TCS SP8 confocal system using a 63x oil-immersion objective.

Serum preparation and biochemical analyses

Following sacrifice, the blood samples were allowed to stand at room temperature for 1–2 h, centrifuged at 4,000 g for 10 min to separate the serum from the other components of blood. The yellowish supernatant of the upper layer of the separated serum was aspirated using a pipette and stored at –80°C for further analysis. For serum lipid analysis, the concentrations of TG and TC in the mouse serum were determined using commercial kits (Applygen, Cat# E1003 for TG; Applygen, Cat# E1005 for TC). To evaluate liver function, the serum levels of alanine aminotransferase (ALT), aspartate aminotransferase (AST), and albumin were analyzed following the protocols provided with the kits (Nanjing Jiancheng, Cat# C009-2-1 for ALT; Nanjing Jiancheng, Cat# C010-2-1 for AST; Nanjing Jiancheng, Cat# A028-2-1 for albumin). Ketone bodies were assessed using a commercial ketone body assay kit (Beijing Boxbio Science & Technology Co., Ltd., Cat# AKCO021M).

Biochemical analyses liver tissue from mice

For the quantification of hepatic TG and TC, 40 mg snap-frozen liver tissue from each mouse was homogenized in PBS. The TG assay kit (Applygen; Cat# E1025) and TC assay kit (Applygen; Cat# E1015) were used to measure the concentrations of hepatic TG and TC following the manufacturer's instructions. The collagen content in the mouse liver was determined by measuring the level of hydroxyproline (HYP) using the HYP assay kit from Solarbio (Cat# BC0250) according to the manufacturer's protocol.

VLDL secretion assay

The C57BL/6J male mice (6–8 weeks old) were injected with PBS, GalNAc-siNC, or GalNAc-si*Plin2* and then fed with a HFD for 7 days. Subsequently, the mice were subjected to a VLDL secretion assay. After a 4-h fast, the mice were injected with tyloxapol (Macklin; Cat# T818533) at a dose of 500 mg/kg of their body weight via the tail vein. Blood samples were collected at the indicated time points, and the serum was separated by centrifugation. The measurement of serum TG measurement was performed as described above.

Treatment with lomitapide

The HFD-induced MASLD mice were administered 1 mg/kg lomitapide (MedChemExpress; Cat# HY-14667) once daily via oral gavage at the beginning of the dark cycle. Three days after the first lomitapide treatment, the mice were injected with PBS, GalNAc-siNC, or GalNAc-si*Plin2*. Six weeks following the injection, the mice were sacrificed, and samples were collected for analysis.

Cold treatment

The HFD-induced MASLD mice were treated with PBS, GalNAc-siNC, or GalNAc-si*Plin2* for 6 weeks. Following the 6-week treatment period, a cold tolerance test was performed. During the test, the mice were placed in a cold chamber set at 4°C for a maximum of 3 h, with unrestricted access to food and water. The body temperature of treated mice was measured hourly using a rectal probe connected to a digital thermometer (Yellow Spring Instruments).

Glucose tolerance and insulin tolerance test

The HFD-induced MASLD mice were treated with either PBS, GalNAc-siNC or GalNAc-si*Plin2*. After 4 weeks of treatment, the mice were subjected to a glucose tolerance test (GTT) to evaluate their glucose metabolism. Mice were fasted overnight and given free access to water. Blood glucose levels were measured by tail bleeding using a glucometer (Roche, NC) at 0, 15, 30, 45, 60, and 120 min after glucose injection (2 g/kg body weight).

Six weeks after siRNA treatment, the MASLD mice were subjected to an insulin tolerance test (ITT) to assess their insulin sensitivity. Mice were fasted for 4 h and insulin were administered intraperitoneally (0.75 U/kg body weight). Blood glucose levels were measured at the indicated time points.

Analysis of atherosclerotic plaque

Groups of mice received treatment were induced by HFD and given PBS, GalNAc-siNC, or GalNAc-si*Plin2*. At the endpoint, mice were sacrificed and perfused with PBS and 4% PFA sequentially. Then the entire aortic trees were isolated and fixed further with 4% PFA for at least 24 h. After the fixation period, any adhering fatty tissue on the outer surface of the aortic trees was removed thoroughly and the aortic trees were subjected to Oil red O staining.

Sirius red staining

Paraffin sections were dewaxed and hydrated with PBS. Collagens were visualized through staining with a modified Sirius red stain kit (Solarbio, Cat# G1472-2) according to manufacturer's instructions. After rinsing with water, the tissue sections were dehydrated with graded ethanol and mounted for examination under bright-field microscopy.

Image acquisition, analysis, and quantification

Section images were acquired with either a Leica TCS SP8 confocal system (63x oil-immersion objective) or a Leica DM IL LED microscope (40x objective). Minor image adjustments (brightness and/or contrast) were performed in Adobe Photoshop CS5. The figures were assembled in Adobe Illustrator CC. For a quantitative analysis of the staining areas of Oil red O, F4/80, or Sirius red, the percentages of positively stained regions were measured using the NIH ImageJ software.

Statistical analysis

All data were subjected to suitable statistical analysis methods. A minimal of three biological replicates was included in every statistical analysis, while standard physiological assays, including plasma lipid measurements, typically involved 4–6 mice. The results were shown as the mean ± SEM as indicated in the corresponding figure legends. The

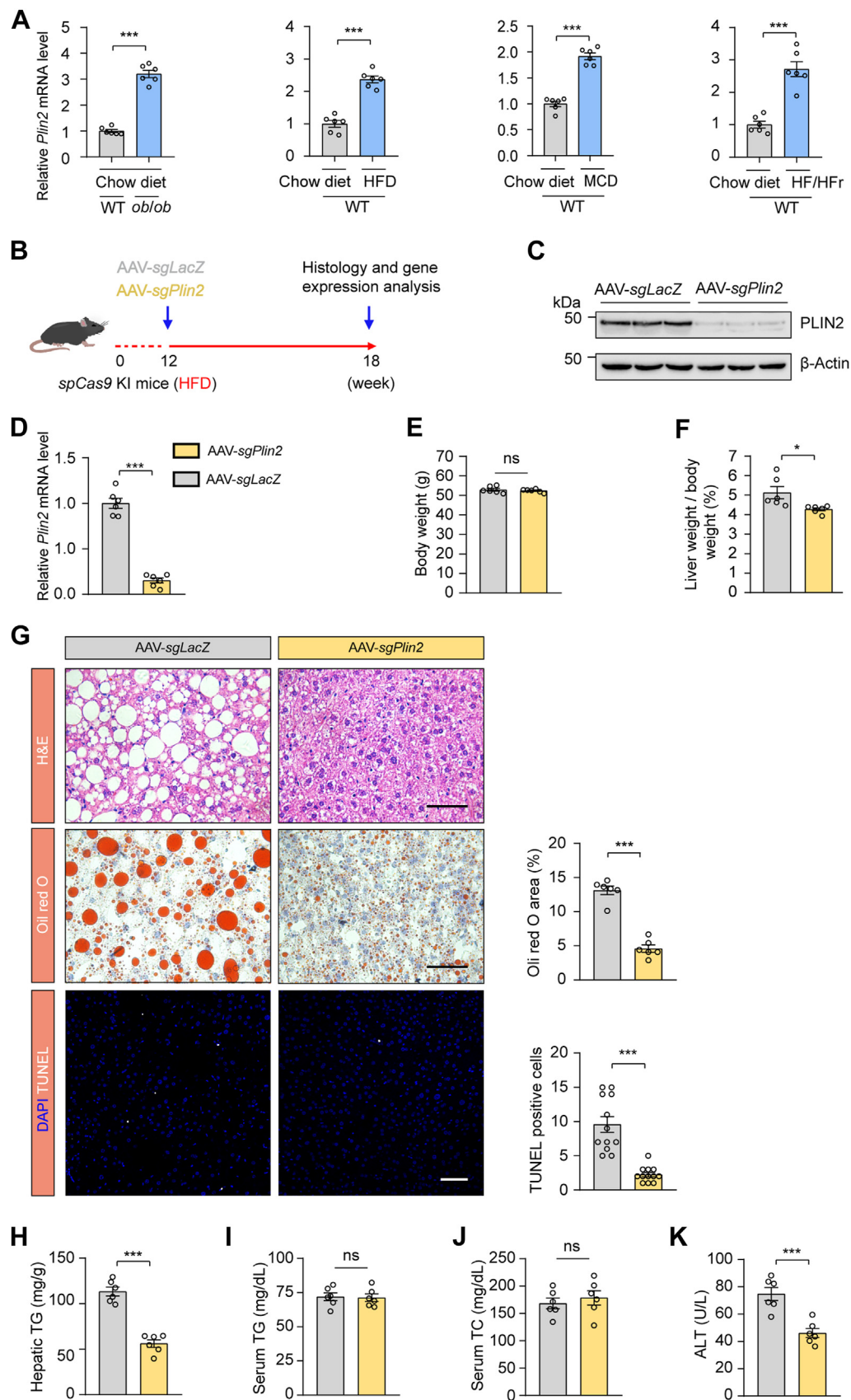


Fig. 1. *Plin2* is a potential therapeutic target for MASLD. A: RT-PCR analysis of relative mRNA levels of hepatic *Plin2* in *ob/ob* mice and C57/BL6J mice subjected to HFD, MCD, or HFD/HFr diet. B: Schematic representation of the procedure for HFD-induced MASLD in *spCas9* KI mice subjected to AAV-mediated gene editing. C: Immunoblotting analysis of hepatic PLIN2 protein levels in HFD-induced MASLD mice subjected to AAV-mediated gene editing. D: RT-PCR analysis of relative mRNA levels of hepatic *Plin2*

statistical software Graphpad Prism 8 (GraphPad Software, La Jolla, CA) was used for conducting statistical analyses. Statistical significance was determined using either a two-tailed Student's *t* test or a one-way ANOVA test, followed by Tukey's multiple comparison tests, as indicated in the figure legends. A result was considered statistically significant if *P* value was less than 0.05. Asterisks denote corresponding statistical significance: * for *P* < 0.05, ** for *P* < 0.01, and *** for *P* < 0.001. For mouse experiments, "n" refers to the number of mice used in the study. For cellular experiments, "n" indicates the number of independent experimental repeats. No data were excluded from the study during the final statistical analysis. A randomization process was performed in grouping mice with identical phenotypes.

RESULTS

Plin2 is an effective and safe drug target for the treatment of MASLD

To thoroughly investigate the complex pathogenesis of MASLD, which presents with a range of pathological features, we utilized both nutritional and genetic induction methods to generate a series of mouse models that reflect the heterogeneity observed in human MASLD patients. Our comprehensive analysis revealed an upregulation in *Plin2*/PLIN2 at both the mRNA and protein levels across these established MASLD mouse models (Fig. 1A and supplemental Fig. S1A). This finding suggests that *Plin2*/PLIN2 may be a common pathogenic factor across various forms of MASLD. Notably, recent studies, including those from our group, have demonstrated that *Plin2* deficiency is linked to resistance to hepatic steatosis in MASLD (16–18). These results highlight the critical role of *Plin2* in MASLD development and suggest its potential as a therapeutic target.

To assess the therapeutic potential of *Plin2* as a drug target, we selectively ablated *Plin2* in the liver of an established MASLD mouse model and evaluated the subsequent effects. We used a mouse strain carrying a "silent" *spCas9* transgene (22) and fed them a HFD for 12 weeks to induce MASLD. We then administered an AAV containing a hepatocyte-specific Cre recombinase, designed to activate the "silent" *spCas9*, along with a guide RNA (gRNA) targeting *Plin2* to specifically deactivate *Plin2* in the liver (supplemental Fig. S1B). The mice were sacrificed for analysis 6 weeks after AAV delivery (Fig. 1B). The gRNA targeting *Plin2* effectively suppressed hepatic *Plin2* expression, as

confirmed by immunoblotting (Fig. 1C) and RT-qPCR (Fig. 1D). Significantly, without affecting body weight, the inactivation of hepatic *Plin2* markedly reduced liver weight to body weight ratio compared to control mice treated with *sgLacZ* (Fig. 1E, F), indicating an improvement in MASLD. Moreover, the characteristic hepatic steatosis of MASLD was significantly alleviated in mice receiving gRNA targeting *Plin2*, as demonstrated by H&E staining and Oil red O staining (Fig. 1G). Consistently, hepatic TG levels in these mice were reduced by approximately 60% (Fig. 1H), while hepatic TC, serum TG and serum TC levels remained comparable between the two groups (supplemental Fig. S1C and Fig. 1I, J).

Chronic steatosis can lead to lipotoxicity and endoplasmic reticulum stress, causing liver injury, which is a key component in the pathogenesis of MASH (24). TUNEL staining revealed a significant decrease in the number of apoptotic cells following *Plin2* deactivation (Fig. 1G). Furthermore, we examined the levels of ALT and AST, two biomarkers commonly used to evaluate liver injury. As expected, the level of ALT was significantly reduced in *Plin2*-knockout mice (Fig. 1K), while the AST level remained unchanged (supplemental Fig. S1D). Additionally, we conducted *Plin2* knockout in the same mouse strain fed a regular chow diet (supplemental Fig. S2A, B). Our results showed that, on a chow diet, *Plin2*-knockout mice had normal body weight and lipid content, with only a modest reduction in hepatic TG levels (supplemental Fig. S2C–I). Importantly, elimination of *Plin2* did not lead to liver injury (supplemental Fig. S2E, J, K). Taken together, these findings indicate that genetic inhibition of *Plin2* in the liver is sufficient to reverse the hepatic steatosis and injury in an established MASLD mouse model, reinforcing the potential of *Plin2* as an effective and safe therapeutic target for the treatment of MASLD.

The enduring effect and reliable biosafety profile of GalNAc-siPlin2

Having identified *Plin2* as a promising therapeutic target for the treatment of MASLD, we developed an siRNA therapy aimed at the pharmacological inhibition of *Plin2* expression. We designed siRNAs to target the evolutionarily conserved regions of both mouse *Plin2* and human *PLIN2* mRNA, resulting in five pairs of candidate siRNAs (supplemental Table S2). We evaluated the efficacy of these siRNA agents in mouse

in HFD-induced MASLD mice subjected to AAV-mediated gene editing. E,F: Body weight (E) and liver-to-body weight ratio (F) for HFD-induced MASLD mice subjected to AAV-mediated gene editing. G: Histological analysis of liver sections from HFD-induced MASLD mice subjected to AAV-mediated gene editing. Quantification of Oil red O staining-positive areas and TUNEL-positive cells is shown. Scale bar, 50 μ m. H,J: Levels of hepatic TG (H), serum TG (I), and serum TC (J) in HFD-induced MASLD mice subjected to AAV-mediated gene editing. K: Levels of serum ALT in HFD-induced MASLD mice subjected to AAV-mediated gene editing. Data are shown as mean \pm SEM. For all panels, n = 6 mice per group. *P* values were determined using a two-tailed Student's *t* test. "ns" denotes no significant difference. **P* < 0.05, ***P* < 0.01, and ****P* < 0.001. AAV, adeno-associated virus; ALT, alanine aminotransferase; HFD, high-fat diet; HFr, high fructose; KI, knockin; MASLD, metabolic dysfunction-associated steatotic liver disease; MCD, methionine-choline deficient; TC, total cholesterol; TG, triglyceride.

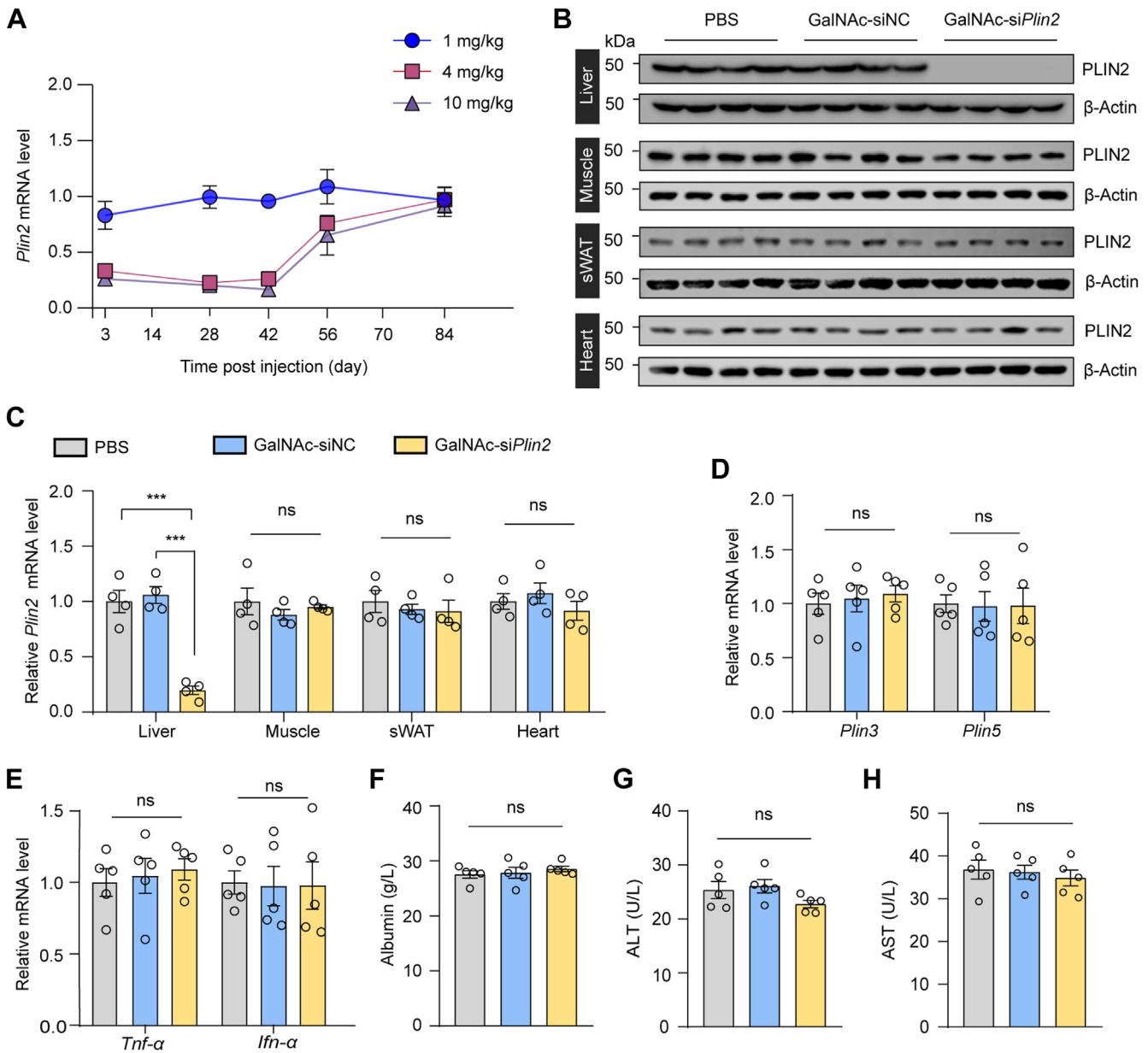


Fig. 2. Treatment with GalNac-siPlin2 reduces hepatic PLIN2 levels and exhibits a biosafety profile. **A:** C57/BL6J mice were subcutaneously injected with indicated doses of GalNac-siPlin2, GalNac-siNC, or an equivalent volume of PBS. Liver tissues were collected at indicated time points postinjection, and the relative mRNA levels of hepatic *Plin2* were evaluated through RT-qPCR analyses. **B,C:** The knockdown efficacy of GalNac-siPlin2 in mouse liver tissues was determined by immunoblotting (**B**) and RT-qPCR analyses (**C**). Muscle, sWAT, and heart were used as negative controls to assess the tissue specificity of GalNac-siPlin2. **D,E:** RT-qPCR analysis of relative mRNA levels of hepatic *Plin3* and *Plin5* genes (**D**) and inflammation-related genes (**E**) in C57/BL6J mice subcutaneously injected with 4 mg/kg GalNac-siPlin2, GalNac-siNC, or PBS. **F-H:** Levels of serum albumin (**F**), serum ALT (**G**), and serum AST (**H**) in C57/BL6J mice subcutaneously injected with 4 mg/kg GalNac-siPlin2, GalNac-siNC, or PBS. Data are shown as mean \pm SEM. $n = 4$ mice per group for panels (**A** and **C**). $n = 5$ mice per group for panels (**D**–**H**). *P* values were determined using one-way ANOVA, followed by Tukey's multiple comparison tests. "ns" denotes no significant difference. **P* < 0.05, ***P* < 0.01, and ****P* < 0.001. ALT, alanine aminotransferase; AST, aspartate aminotransferase; GalNac, N-acetylgalactosamine; RT-qPCR, quantitative real-time PCR; sWAT, subcutaneous white adipose tissue.

AML12 and human HepG2 cells. Our results indicated that the first three pairs of siRNA agents exhibited superior activity (supplemental Fig. S3A–D). Notably, owing to a lower number of base-pair mismatches, the second and third pairs of siRNA agents were selected for further investigation.

We subjected the mouse-targeted siRNA agents to chemical modifications, including the addition of 2'-methoxy group, 2'-fluoro, and phosphorothioate linkages, using an advanced stabilization chemistry pattern to enhance stability and reduce immunogenicity (25, 26). The modified siRNA agents were subsequently

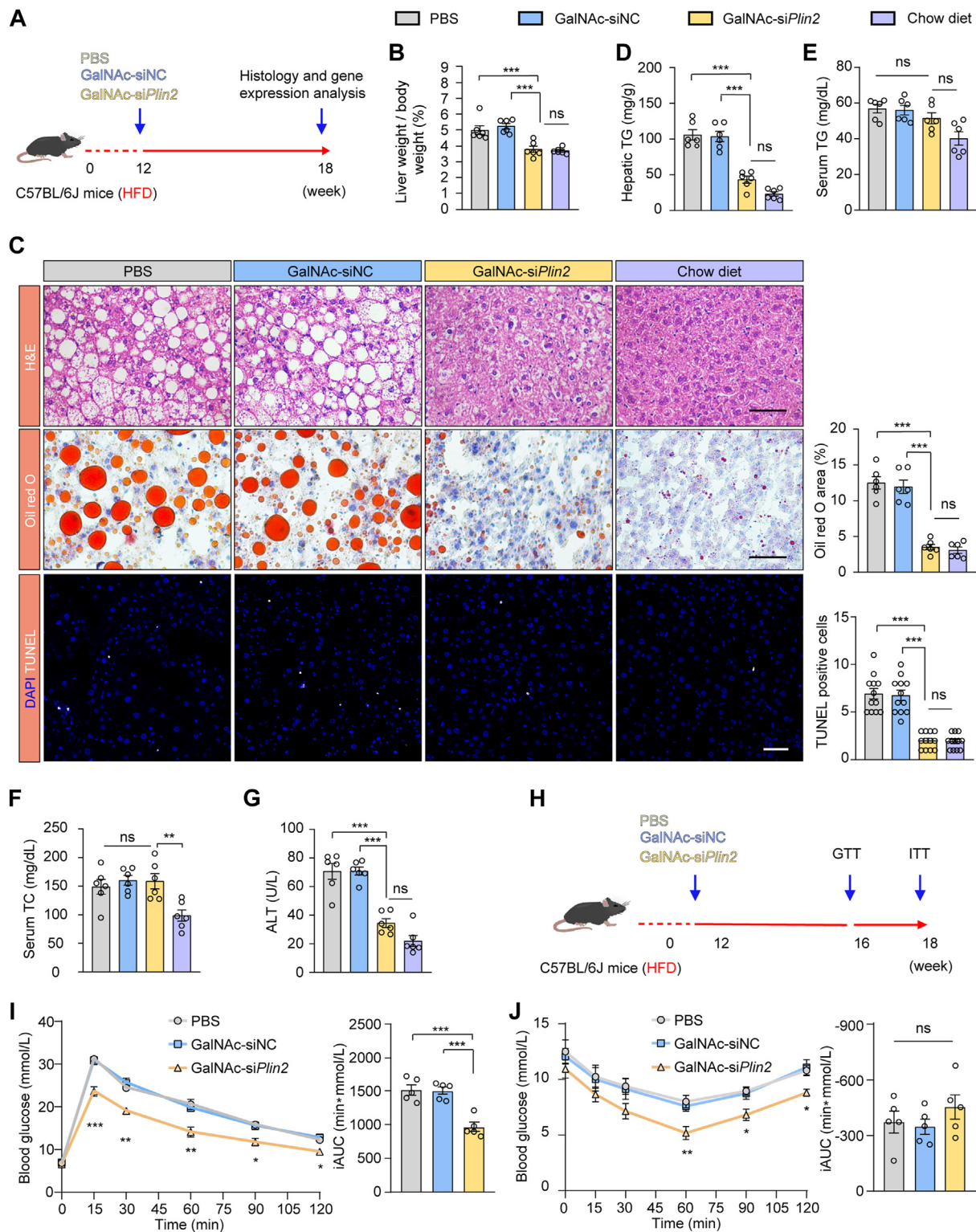


Fig. 3. Treatment with GalNac-siPlin2 ameliorates MASLD induced by HFD. **A:** Schematic representation of the HFD-induced MASLD in C57BL/6J mice subcutaneously injected with 4 mg/kg GalNac-siPlin2, GalNac-siNC, or PBS. Mice fed with a chow diet serve as the healthy control. **B:** The liver-to-body weight ratio for chow diet-fed mice and HFD-induced MASLD mice subcutaneously injected with 4 mg/kg GalNac-siPlin2, GalNac-siNC, or PBS. **C:** Histological analysis of liver sections from chow diet-fed mice and HFD-induced MASLD mice subcutaneously injected with 4 mg/kg GalNac-siPlin2, GalNac-siNC, or PBS. Quantification of Oil red O staining-positive areas and TUNEL-positive cells is shown. Scale bar, 50 μ m. **D-G:** Levels of hepatic TG (**D**), serum TG (**E**), serum TC (**F**), and serum ALT (**G**) from chow diet-fed mice and HFD-induced MASLD mice subcutaneously injected with 4 mg/kg GalNac-siPlin2, GalNac-siNC, or PBS. **H:** Schematic illustration of the GTT and ITT experimental procedures. **I,J:** Assessment of glucose tolerance and insulin sensitivity in HFD-induced MASLD mice subcutaneously injected with 4 mg/kg GalNac-siPlin2, GalNac-siNC, or PBS. The incremental area under the curve (iAUC_{0-120 min}) was quantified. Data are shown as mean \pm SEM. n = 6

named *siPlin2-2* ST and *siPlin2-3* ST, respectively. Following modification, we demonstrated that the mouse-targeted siRNA agents maintained their ability to effectively repress *Plin2* expression (supplemental Fig. S3E, F). We then generated IC₅₀ curves for both siRNA agents, showing that *siPlin2-2* ST had greater potency in inhibiting *Plin2*, with an IC₅₀ value of approximately 0.3085 nM (supplemental Fig. S3G). Consequently, *siPlin2-2* ST was selected for further in vivo study and was subsequently conjugated with N-acetylgalactosamine (GalNAc). This GalNAc moiety facilitates hepatocyte entry by interacting with the membrane protein asialoglycoprotein receptor (supplemental Fig. S3H) (27). The resulting mouse-targeted siRNA agent for in vivo use was named GalNAc-*siPlin2*, while its corresponding human-targeted counterpart was called GalNAc-*siPLIN2*.

To evaluate the pharmacodynamics of GalNAc-*siPlin2*, we administered a single subcutaneous injection of 1, 4, or 10 mg/kg GalNAc-*siPlin2* or PBS as control to mice. Inhibition of *Plin2* was detectable by day 3 postinjection. Specifically, at week 4 following the injection, the expression levels of hepatic *Plin2* were reduced to 99.5 ± 0.2%, 22.6 ± 0.1% and 20.1 ± 0.1% with 1, 4, or 10 mg/kg GalNAc-*siPlin2*, respectively, compared to the control group (Fig. 2A). Furthermore, the suppression of *Plin2* expression levels remained significant at week 6, with levels remaining below 30% in mice treated with 4 and 10 mg/kg GalNAc-*siPlin2* (Fig. 2A). By the end of the study (week 12), the expression level of *Plin2* had almost returned to that of the control group. Considering both drug dosage and efficacy, the 4 mg/kg dose of the siRNA agent was chosen for subsequent studies. We further analyzed the tissue specificity and gene specificity of GalNAc-*siPlin2*. Remarkably, GalNAc-*siPlin2* did not affect *Plin2* expression in muscle, sWAT or heart in mice (Fig. 2B, C), and it did not alter the expression of *Plin3* or *Plin5* (Fig. 2D), two other PAT family members in the liver. These results collectively demonstrate that GalNAc-*siPlin2* has high potency, a prolonged duration of action, and specificity.

Additionally, we conducted a comprehensive evaluation of the potential toxicity associated with GalNAc-*siPlin2*. It is known that siRNA agents may trigger the innate immune response, leading to increased levels of inflammatory cytokines, particularly TNF-α and IFN-α (28). However, our RT-qPCR results did not show elevated expression of these two genes (Fig. 2E), suggesting minimal or no activation of the innate immune system. Moreover, we assessed serum albumin, ALT, and AST, three biomarkers commonly used to indicate liver

injury. Our findings indicated that GalNAc-*siPlin2* did not change the levels of these biomarkers compared to controls (Fig. 2F–H). Histological analyses also showed no discernible histological or structural abnormalities in the heart, liver, spleen, lung, or kidney when compared to control mice (supplemental Fig. S4A). Furthermore, no significant changes in major organ indexes were observed (supplemental Fig. S4B). Additionally, we analyzed lipid content and fasting blood glucose levels. Apart from a slight reduction in hepatic TG (supplemental Fig. S4C), GalNAc-*siPlin2* did not have any significant effect on these parameters compared to the controls (supplemental Fig. S4D–G). In summary, the physiological and biochemical data collectively demonstrate that GalNAc-*siPlin2* is well tolerated and exhibits no significant side effects.

GalNAc-*siPlin2* attenuates hepatic steatosis and injury in MASLD induced by nutritional and genetic factors

To evaluate the in vivo efficacy of GalNAc-*siPlin2*, we used an HFD-induced MASLD model (Fig. 3A). Six weeks postinjection, GalNAc-*siPlin2* still silenced *Plin2* expression by over 90% (supplemental Fig. S5A, B). Notably, compared to the control group, GalNAc-*siPlin2* significantly reduced the liver-to-body weight ratio (Fig. 3B), nearly restoring it to the levels seen in mice on a standard chow diet, without influencing overall body weight (supplemental Fig. S5C). We further assessed steatosis through H&E and Oil red O staining, which showed a marked reduction in hepatic LDs in GalNAc-*siPlin2*-treated mice (Fig. 3C). Consistent with these observations, hepatic TG levels were reduced by nearly 60%, with no significant effect on serum TG and serum TC levels (Fig. 3D–F). However, hepatic TC levels remained unchanged (supplemental Fig. S5D).

Encouraged by these findings, we investigated whether GalNAc-*siPlin2* could mitigate liver injury. TUNEL staining indicated a reduction in apoptotic cells following GalNAc-*siPlin2* treatment (Fig. 3C). Additionally, ALT levels were normalized in the GalNAc-*siPlin2*-treated group (Fig. 3G), while AST levels in HFD-fed mice remained comparable to those in mice fed on a chow diet (supplemental Fig. S5E). These results collectively demonstrate the hepato-protective effects of GalNAc-*siPlin2*.

Considering the established link between hepatic steatosis and insulin resistance, and the strong association between MASLD and T2D (29), we investigated the potential of GalNAc-*siPlin2* to improve glucose metabolism in MASLD mice (Fig. 3H). GTTs and ITTs showed improved glucose intolerance and insulin

mice per group for panels (A–G), n = 5 mice per group for panels (I and J). *P* values were determined using one-way ANOVA followed by Tukey's multiple comparison tests. "ns" denotes no significant difference. **P* < 0.05, ***P* < 0.01, and ****P* < 0.001. ALT, alanine aminotransferase; GalNAc, N-acetylgalactosamine; GTT, glucose tolerance test; HFD, high-fat diet; ITT, insulin tolerance test; MASLD, metabolic dysfunction-associated steatotic liver disease; TC, total cholesterol; TG, triglyceride.

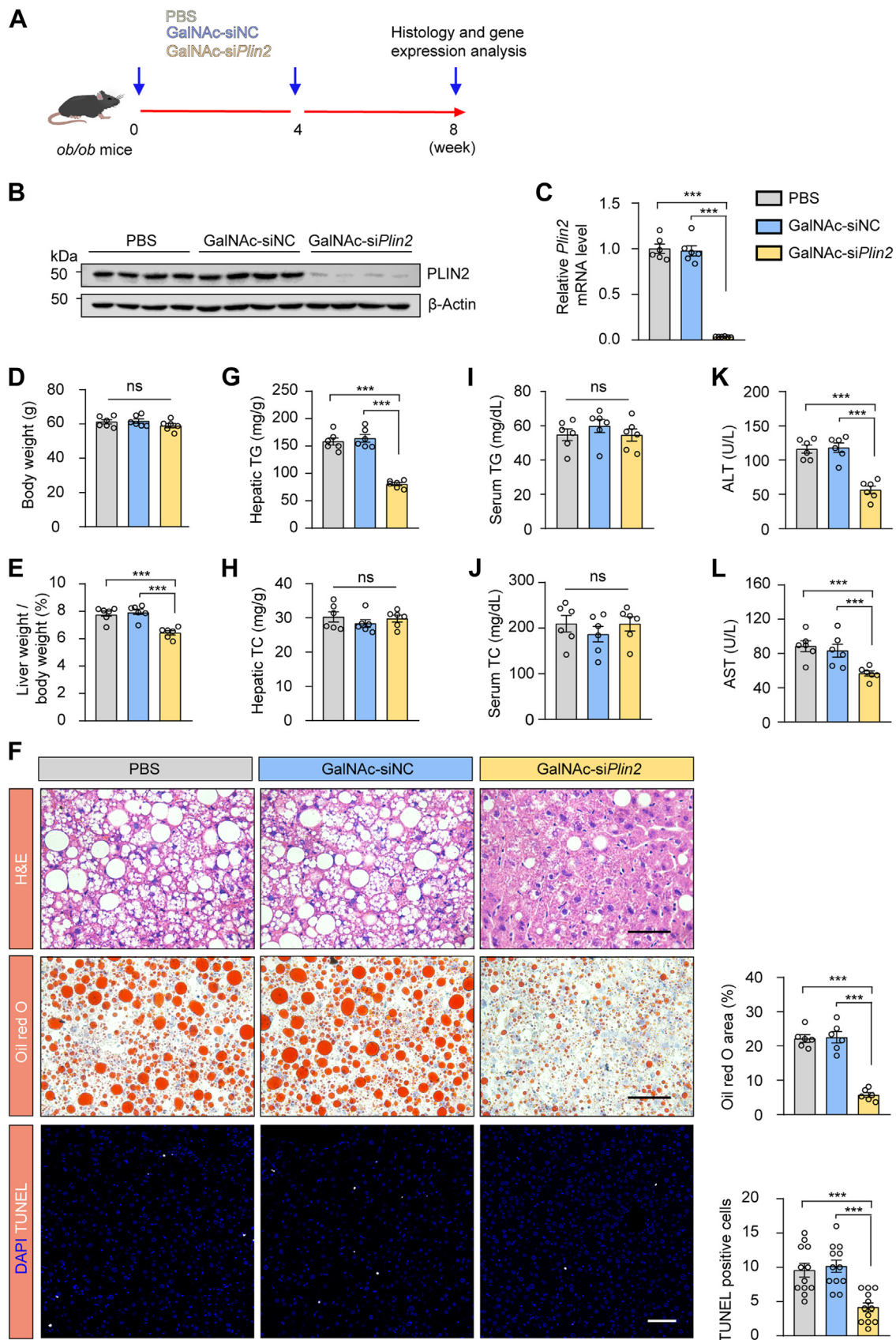


Fig. 4. Treatment with GalNAc-si*Plin2* ameliorates MASLD induced by obesity. A; Schematic representation of obesity-induced MASLD in leptin-deficient (*ob/ob*) mice subcutaneously injected with 4 mg/kg GalNAc-si*Plin2*, GalNAc-siNC, or PBS. B: RT-qPCR analysis of relative mRNA levels of hepatic *Plin2* in *ob/ob* mice subcutaneously injected with 4 mg/kg GalNAc-si*Plin2*, GalNAc-siNC, or PBS. C: Immunoblotting analysis of hepatic PLIN2 protein levels in *ob/ob* mice subcutaneously injected with 4 mg/kg

sensitivity in GalNAc-si*Plin2*-treated mice compared to controls (Fig. 3I, J). Although fasting blood glucose levels showed minimal changes at weeks 4 and 6 post-treatment (supplemental Fig. S5F, G), the improvements in GTT and ITT further support the beneficial effects of GalNAc-si*Plin2* on glucose metabolism in MASLD mice.

We subsequently administered GalNAc-si*Plin2* to adult leptin-deficient *ob/ob* mice (Fig. 4A), a well-established genetic MASLD model. GalNAc-si*Plin2* efficiently repressed hepatic *Plin2* expression (Fig. 4B, C). Consistent with the results from HFD-fed mice, body weight was unaffected, while the liver-to-body weight ratio and hepatic TG levels were significantly reduced after GalNAc-si*Plin2* treatment (Fig. 4D–G). Hepatic TC, serum TG, and serum TC levels remained unchanged (Fig. 4H–J). Moreover, we observed a reduction in apoptotic cells following GalNAc-si*Plin2* treatment (Fig. 4F), suggesting a protective effect against liver injury. Additionally, both ALT and AST levels were reduced by GalNAc-si*Plin2* treatment (Fig. 4K, L). Collectively, these results strongly support the therapeutic efficacy of GalNAc-si*Plin2* in both the HFD-induced MASLD model and *ob/ob* mouse model, highlighting its potential as a promising therapeutic intervention for MASLD.

GalNAc-si*Plin2* enhances hepatic VLDL-TG secretion to ameliorates MASLD

Hepatic steatosis is closely linked to the dysregulation of lipogenesis, lipolysis, fatty acid β oxidation, and VLDL secretion (2). To elucidate the molecular mechanisms through which GalNAc-si*Plin2* exerts its beneficial effects of on HFD-induced MASLD, we initially conducted a comprehensive analysis of hepatic TG metabolism using RT-qPCR analysis. Contrary to our expectations, no significant alterations were observed in the transcriptional levels of genes related to lipogenesis, lipolysis, or β -oxidation (supplemental Fig. S6A–C). Consistently, the levels of ketone bodies, which are products of hepatic fatty acid oxidation, were not changed (supplemental Fig. S6D). To determine whether hepatic *Plin2* knockdown activates autophagy, we evaluated the ratios of LC3B-I to LC3B-II, a widely used marker of autophagosomes. However, we did not detect any conversion from LC3B-I to LC3B-II at week

6 posttreatment with GalNAc-si*Plin2* (supplemental Fig. S6E). Furthermore, there were no changes in fatty acid oxidation or autophagy of the liver throughout the course of GalNAc-si*Plin2* treatment (supplemental Fig. S6F–M). Subsequently, we investigated the potential influence of GalNAc-si*Plin2* on VLDL secretion following the inhibition of lipase activity with tyloxapol. Our results indicated an increased secretion of VLDL-TG in the GalNAc-si*Plin2*-treated group (Fig. 5A), implying that GalNAc-si*Plin2* may alleviate hepatic steatosis, at least in part, through the acceleration of hepatic VLDL-TG secretion. Consistent with this finding, the expression of microsomal TG transfer protein (MTP), which is crucial for the translocation of newly synthesized APOB100 to the endoplasmic reticulum and the assembly of primordial VLDL particles, was found to be upregulated (Fig. 5B), further supporting the aforementioned hypothesis.

To corroborate this hypothesis, we used lomitapide, a potent MTP inhibitor, to block VLDL secretion. Consistent with the well-established role of MTP in mediating physiological hepatic VLDL secretion, lomitapide treatment led to a reduction in VLDL secretion (supplemental Fig. S6N) and a decrease in plasma TG and TC levels (supplemental Fig. S6O). Thereafter, we used lomitapide to block VLDL secretion in mice treated with PBS, GalNAc-siNC, or GalNAc-si*Plin2*. Notably, no significance changes in body weight or liver weight were observed in the GalNAc-si*Plin2*-treated group (Fig. 5C, D). As anticipated, the therapeutic effect of GalNAc-si*Plin2* in mitigating hepatic steatosis was abolished (Fig. 5E–H). Moreover, the number of TUNEL-positive cells remained unchanged in mice treated with GalNAc-si*Plin2* (Fig. 5E), and no improvements in ALT levels were detected (Fig. 5I). Collectively, these data suggest that VLDL-TG secretion is essential for the therapeutic effects of GalNAc-si*Plin2*.

Given that we did not observe increased serum TG or TC (supplemental Fig. S7A, B) or an elevated risk of atherosclerosis (supplemental Fig. S7C) in HFD-induced MASLD mice treated with GalNAc-si*Plin2*, we speculated that the secreted lipids might be taken up by peripheral tissues. To investigate this possibility, we analyzed the expression of *CD36* and *Vldl*, two genes implicated in the uptake of free fatty acids and VLDL, respectively, in organs capable of metabolizing

GalNAc-si*Plin2*, GalNAc-siNC, or PBS. D,E: Body weight (D) and liver-to-body weight ratio (E) for *ob/ob* mice subcutaneously injected with 4 mg/kg GalNAc-si*Plin2*, GalNAc-siNC, or PBS. F: Histological analysis of liver sections from *ob/ob* mice subcutaneously injected with 4 mg/kg GalNAc-si*Plin2*, GalNAc-siNC, or PBS. Quantification of Oil red O staining-positive areas and TUNEL-positive cells is shown. Scale bar, 50 μ m. G–J: The levels of hepatic TG (G), hepatic TC (H), serum TG (I), and serum TC (J) from *ob/ob* mice subcutaneously injected with 4 mg/kg GalNAc-si*Plin2*, GalNAc-siNC, or PBS. K,L: The levels of serum ALT (K) and serum AST (L) in *ob/ob* mice subcutaneously injected with 4 mg/kg GalNAc-si*Plin2*, GalNAc-siNC, or PBS. Data are shown as mean \pm SEM. For all the panels, n = 6 mice per group. *P* values were calculated using one-way ANOVA followed by Tukey's multiple comparison tests. "ns" denotes no significant difference. **P* < 0.05, ***P* < 0.01, and ****P* < 0.001. ALT, alanine aminotransferase; AST, aspartate aminotransferase; GalNAc, N-acetylgalactosamine; MASLD, metabolic dysfunction-associated steatotic liver disease; RT-qPCR, quantitative real-time PCR; TC, total cholesterol; TG, triglyceride.

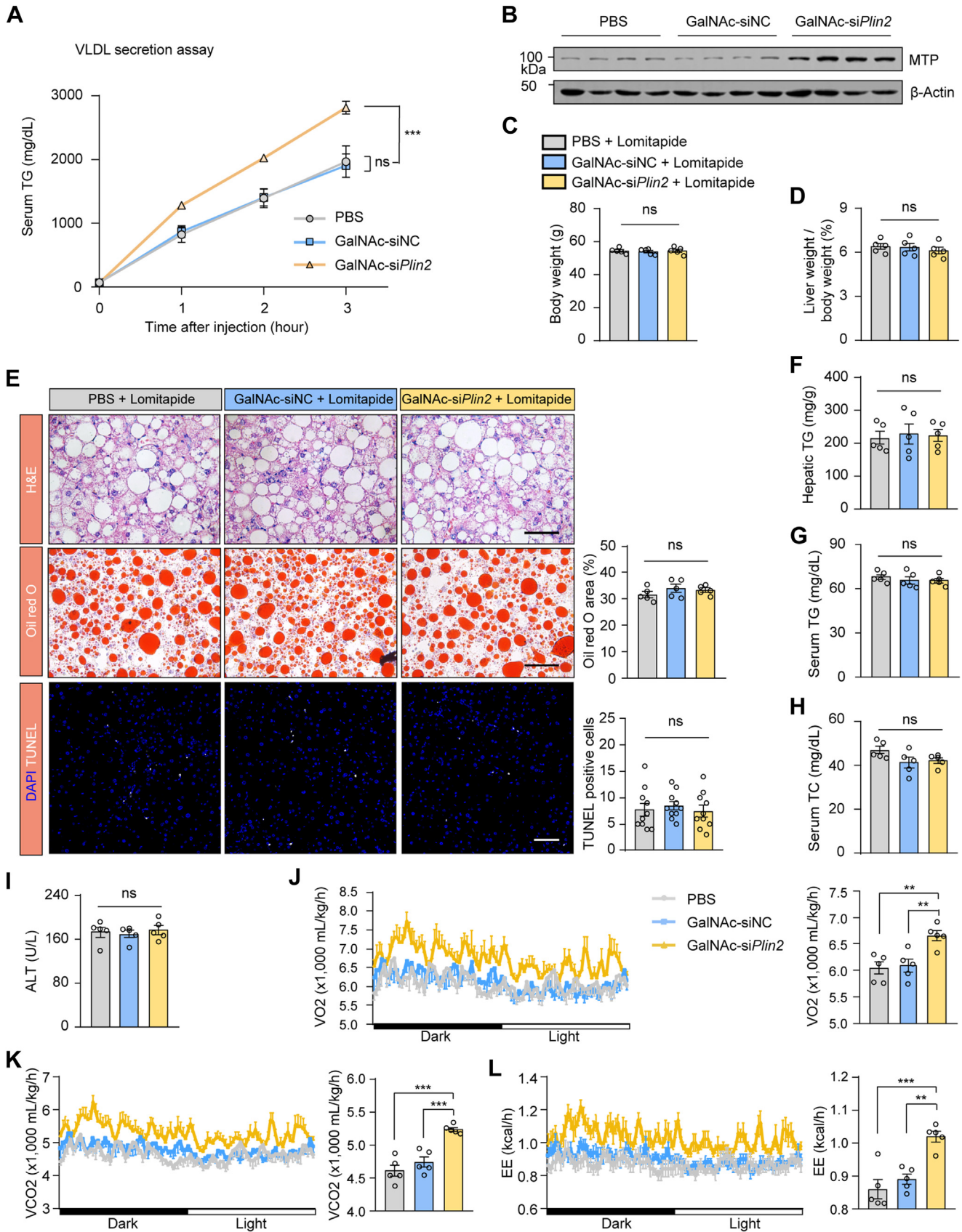


Fig. 5. Treatment with GalNAc-siPlin2 increases the hepatic secretion of VLDL TG. **A:** Treatment with GalNAc-siPlin2 increased the hepatic secretion of VLDL TG. **B:** Immunoblotting of hepatic MTP in HFD-induced MASLD mice subcutaneously injected with 4 mg/kg GalNAc-siPlin2, GalNAc-siNC, or PBS. **C,D:** The body weights (**C**) and the ratios of liver weight to body weight (**D**) in HFD-induced MASLD mice treated with lomitapide, followed by subcutaneous injection of the 4 mg/kg GalNAc-siPlin2, GalNAc-siNC, or PBS.

or storing lipid. RT-qPCR analysis revealed that the expression of *CD36* and *Vldlr* was upregulated in brown adipose tissue (BAT) (supplemental Fig. S7D–G). However, no abnormal lipid accumulation was detected in BAT (supplemental Fig. S7H). These findings support the concept that MASLD is a multisystem disease, and the amelioration of MASLD may confer benefits to glycometabolism and other extrahepatic tissues. Consequently, we assessed the thermogenic activity of BAT and discovered that the expression of thermogenic genes was elevated in the GalNAc-si*Plin2*-treated group (supplemental Fig. S7I). Consistently, these mice displayed increased body temperature during cold exposure (supplemental Fig. S7J), suggesting that thermogenic activity was stimulated. Indeed, metabolic cage analyses revealed that mice receiving GalNAc-si*Plin2* treatment exhibited substantial enhancements in O₂ consumption, CO₂ production, and energy expenditure (Fig. 5J–L). Thus, our results indicate that secreted VLDL-TG from the liver following GalNAc-si*Plin2* treatment acts as a lipid fuel for the activated thermogenesis in BAT.

GalNAc-si*Plin2* ameliorates MASH in mice induced by HFD/HFr diet

Encouraged by the promising therapeutic effects of GalNAc-si*Plin2* on steatosis and liver injury in MASLD models, we expanded our investigation to evaluate its efficacy in managing inflammation and fibrosis, which are critical pathological features of MASH, the progressive form of MASLD. We administered PBS, GalNAc-siNC, or GalNAc-si*Plin2* to mice with MASH induced by an HFD/HFr diet (Fig. 6A) (30). GalNAc-si*Plin2* significantly reduced the expression of *Plin2* and alleviated steatosis and liver injury in the MASH model (supplemental Fig. S8A–G and Fig. 6B–E).

Recognizing the importance of inflammation and fibrosis as pathological indicators of MASH (31, 32), we further investigated the effects of GalNAc-si*Plin2* on these specific aspects. Our analysis revealed a reduction in inflammatory cell infiltration, as evidenced by the reduced presence of macrophages (Fig. 6C). In agreement with these observations, RT-qPCR data showed decreased expression of inflammatory genes in the livers of GalNAc-si*Plin2*-treated

group (Fig. 6F). Additionally, Sirius red staining for fibrosis assessment unveiled a significant reduction in collagen deposition in GalNAc-si*Plin2*-treated mice (Fig. 6C). Concurrently, the amount of HYP, a nonessential amino acid found in collagen, was found to be reduced in this group (supplemental Fig. S8H). RT-qPCR analysis of fibrosis-related genes confirmed these findings, with lower expression levels of *Calla1*, *Acta2*, and *Mmp2* in the GalNAc-si*Plin2*-treated group (Fig. 6G). Taken together, our study demonstrates that GalNAc-si*Plin2* efficiently alleviates steatosis, inflammation and fibrosis in an HFD/HFr diet-induced MASH model in mice, underscoring its potential as a therapeutic agent for the advanced stages of MASLD.

Human-targeted GalNAc-siPLIN2 improves MASH in humanized PLIN2 KI mice

To explore the therapeutic potential of the siRNA agent targeting human *PLIN2* (GalNAc-si*PLIN2*) in MASH, we generated humanized *PLIN2* KI mice by replacing murine *Plin2* gene with the human *PLIN2* gene (supplemental Fig. S9A). The successful humanization of *PLIN2* in these mice was confirmed through genotyping (supplemental Fig. S9B, C), RT-qPCR (supplemental Fig. S9D), and immunoblotting analyses (supplemental Fig. S9E), with comparable expression levels of *Plin2/PLIN2* between WT and humanized mice (supplemental Fig. S9F). Immunofluorescence analysis demonstrated that PLIN2 localized to the surface of LDs in humanized mice, resembling the localization of mouse PLIN2 in WT mice (supplemental Fig. S9G). The humanized mice were subsequently subjected to an HFD/HFr diet to induce MASH, and the model proved susceptible to MASH development (supplemental Fig. S10). The above results validate the successful establishment of humanized *PLIN2* KI mice, providing an appropriate model for evaluating the efficacy of GalNAc-si*PLIN2* in targeting human *PLIN2* for MASH treatment.

Upon administration of PBS, GalNAc-siNC, or GalNAc-si*PLIN2* to HFD/HFr diet-induced humanized MASH mice, GalNAc-si*PLIN2* effectively suppressed *PLIN2* expression, demonstrating potent in vivo activity (supplemental Fig. S11A, B). Consistent with the effects observed in MASH mice with the mouse *Plin2* gene,

E: Blocking hepatic secretion of VLDL TG by lomitapide abolished the effects of GalNAc-si*Plin2* on hepatic steatosis and liver injury. Quantification of Oil red O staining-positive areas and TUNEL-positive cells are shown. Scale bar, 50 μ m. F–I: Levels of hepatic TG (F), serum TG (G), serum TC (H), and serum ALT (I) in HFD-induced MASLD mice treated with lomitapide, followed by subcutaneous injection of 4 mg/kg GalNAc-si*Plin2*, GalNAc-siNC, or PBS. J–L: Oxygen consumption (VO₂) (J), carbon dioxide production (VCO₂) (K), and energy expenditure (EE) (L) in mice treated with 4 mg/kg GalNAc-si*Plin2*, GalNAc-siNC, or PBS at 4°C. Data are shown as mean \pm SEM. For panel (A), n = 4 mice per group, and P values were determined using two-way ANOVA followed by Bonferroni's multiple comparisons test. For panels (C–I), n = 5 mice per group, and P values were calculated using one-way ANOVA followed by Tukey's multiple comparison tests. For panels (J–L), n = 5 mice per group, and P values were calculated using two-way ANOVA followed by Bonferroni's multiple comparisons test or one-way ANOVA followed by Tukey's multiple comparison tests. "ns" denotes no significant difference. ***P < 0.001. ALT, alanine aminotransferase; AST, aspartate aminotransferase; GalNAc, N-acetylgalactosamine; HFD, high-fat diet; MASLD, metabolic dysfunction-associated steatotic liver disease; TC, total cholesterol; TG, triglyceride.

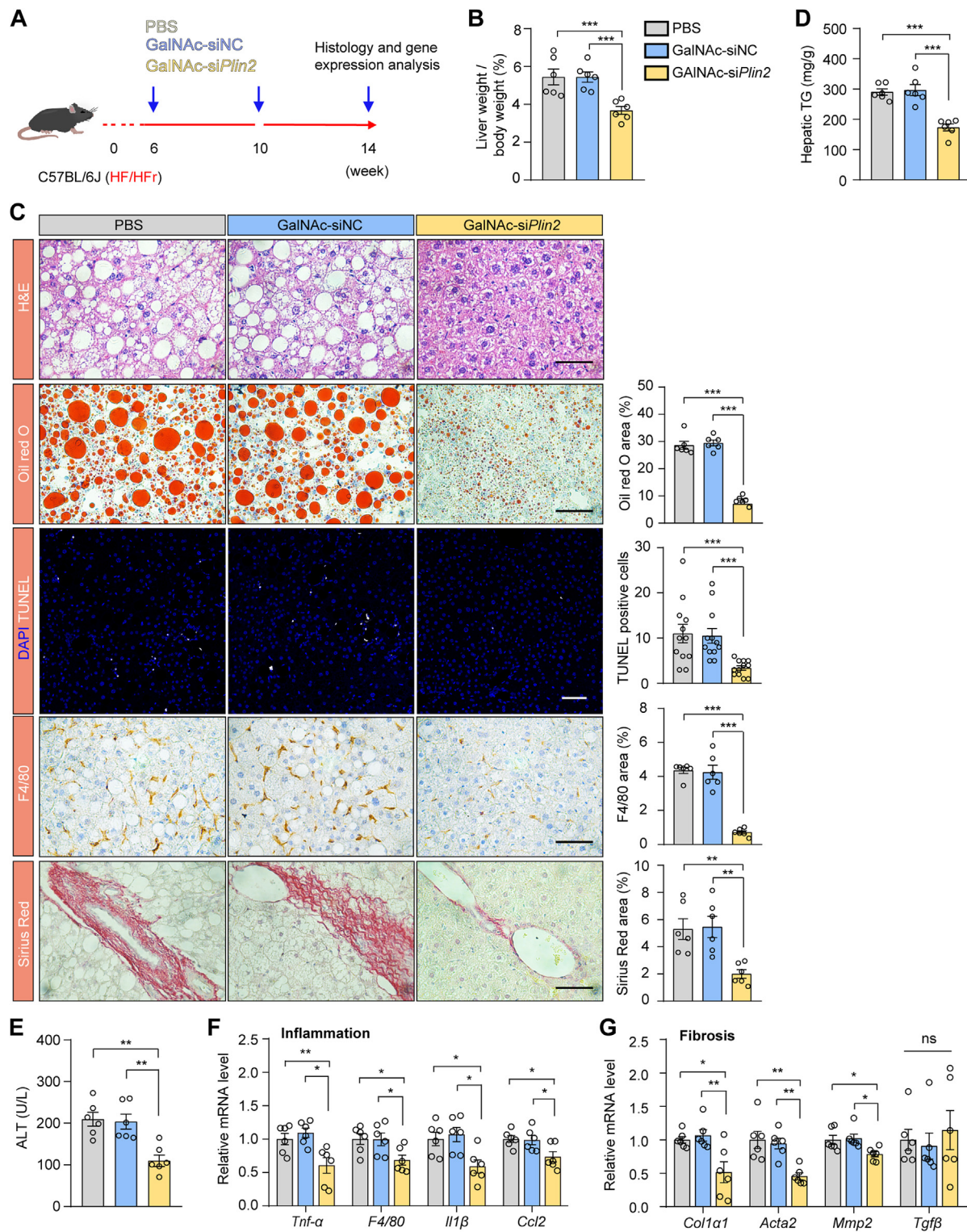


Fig. 6. Treatment with GalNAc-siPlin2 ameliorates inflammation and fibrosis in HFD/HFr diet-induced MASH mice. **A:** Schematic representation of HFD/HFr diet-induced MASH in C57/BL6J mice subcutaneously injected with 4 mg/kg GalNAc-siPlin2, GalNAc-siNC, or PBS. **B:** The liver-to-body weight ratio in HFD/HFr diet-induced MASH mice subcutaneously injected with 4 mg/kg GalNAc-siPlin2, GalNAc-siNC, or PBS. **C:** Histological analysis of liver sections from HFD/HFr diet-induced MASH mice subcutaneously injected with 4 mg/kg GalNAc-siPlin2, GalNAc-siNC, or PBS. Quantification of Oil red O staining-positive areas, TUNEL-positive cells, F4/80-positive areas, and Sirius red staining-positive areas is shown. Scale bar, 50 μ m. **D,E:** Levels of hepatic TG (**D**) and serum ALT (**E**) in HFD/HFr diet-induced MASH mice subcutaneously injected with 4 mg/kg GalNAc-siPlin2, GalNAc-siNC, or PBS. **F,G:** RT-qPCR analysis of relative mRNA levels of inflammation-related genes and fibrosis-related genes (**G**) in liver tissues from HFD/HFr diet-induced MASH mice subcutaneously injected with 4 mg/kg GalNAc-siPlin2, GalNAc-siNC, or PBS. Data are shown as mean \pm SEM. For all panels, n = 6 mice per group. P values are determined using one-way ANOVA followed by Tukey's multiple comparison tests. "ns" denotes no significant difference. *P < 0.05. **P < 0.01. ***P < 0.001. ALT, alanine aminotransferase; GalNAc, N-acetylgalactosamine; HFD/HFr, high-fat diet/high fructose; IHC, immunohistochemistry; MASH, metabolic dysfunction-associated steatohepatitis; RT-qPCR, quantitative real-time PCR.

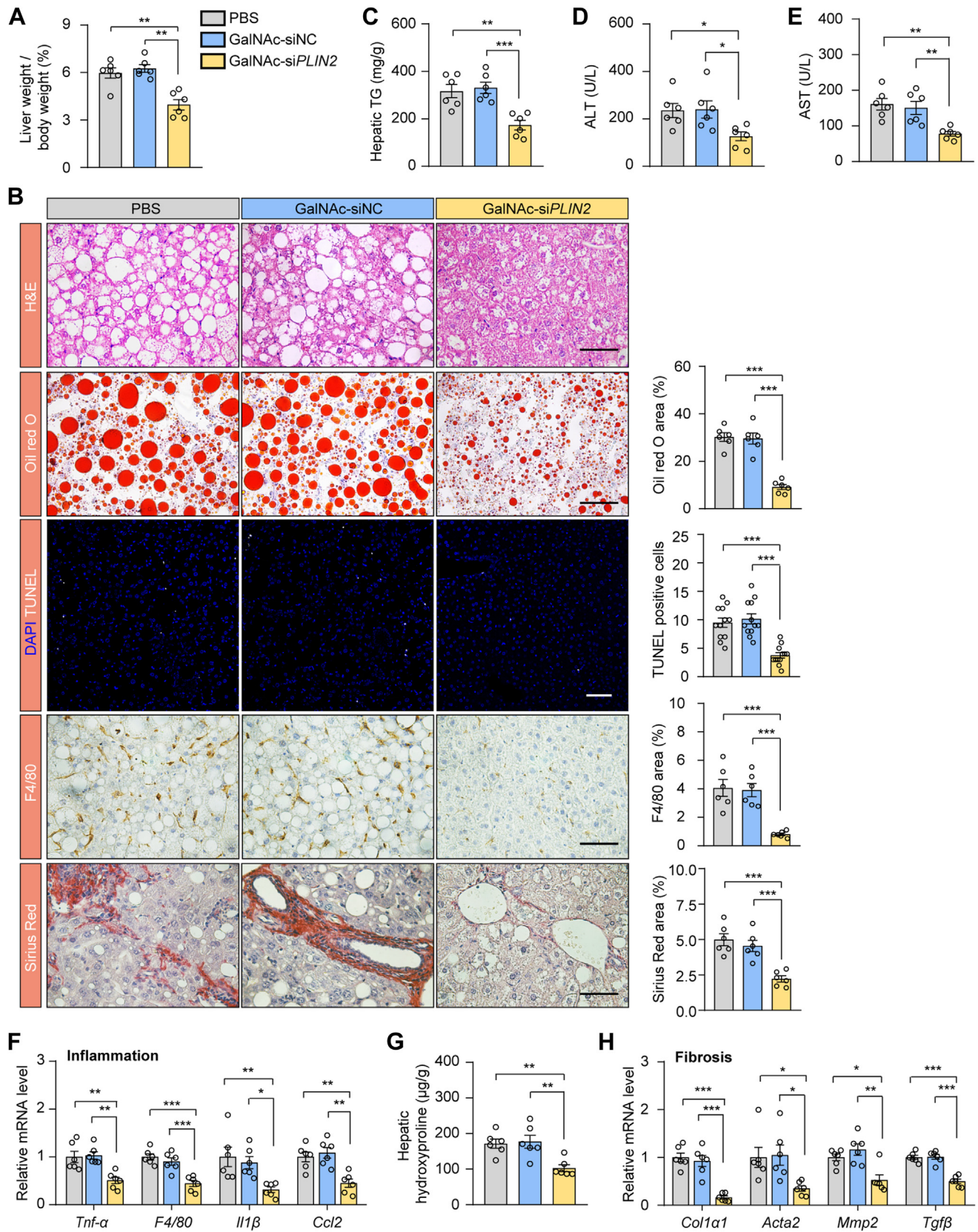


Fig. 7. Treatment with GalNAc-siPLIN2 ameliorates HFD/HFr diet-induced MASH in humanized *PLIN2* knockin mice. **A:** The liver-to-body weight ratios in humanized *PLIN2* knockin mice with HFD/HFr diet-induced MASH, following subcutaneous injection of 4 mg/kg GalNAc-si $Plin2$, GalNAc-siNC, or PBS. **B:** Histological analyses of liver sections from humanized *PLIN2* knockin mice with HFD/HFr diet-induced MASH, following subcutaneous injection of 4 mg/kg GalNAc-si $Plin2$, GalNAc-siNC, or PBS. Quantification of Oil red O staining-positive areas, TUNEL-positive cells, F4/80-positive areas, and Sirius red staining-positive areas are shown.

GalNAc-siPLIN2 treatment reduced the liver-to-body weight ratio without influencing the body weight of humanized MASH mice (Fig. 7A and supplemental Fig. S11C). Histological analysis revealed a significant improvement in hepatic steatosis in mice treated with GalNAc-siPLIN2, as evidenced by diminished LD accumulation compared to controls (Fig. 7B). Additionally, hepatic TG levels decreased in GalNAc-siPLIN2-treated mice (Fig. 7C), while hepatic TC, serum TG, and serum TC remained unchanged among different treatment groups (supplemental Fig. S11D–F). GalNAc-siPLIN2 treatment also led to a decrease in hepatic apoptotic cells, indicative of reduced cell death (Fig. 7B), corroborated by lower serum ALT and AST levels (Fig. 7D, E).

Further investigation into the effects of GalNAc-siPLIN2 on inflammation and fibrosis revealed that GalNAc-siPLIN2 treatment reduced inflammatory infiltration in the livers of treated mice, as detected by macrophage detection and RT-qPCR analyses (Fig. 7B, F). Sirius red staining for fibrosis assessment showed a marked reduction in fibrotic areas in the livers of GalNAc-siPLIN2-treated mice (Fig. 7B). This decrease in fibrosis was further confirmed by reduction in collagen deposition, evidenced by diminished HYP content in liver tissue (Fig. 7G). Consistently, fibrosis-related gene expression levels were downregulated following GalNAc-siPLIN2 treatment (Fig. 7H). Together, these findings support the advancement of GalNAc-siPLIN2 into clinical development for human MASLD/MASH therapy, highlighting its potential as a promising therapeutic strategy. Further investigation in clinical trials is necessary to fully realize its therapeutic benefits.

DISCUSSION

The burgeoning incidence of MASLD poses a significant concern due to its escalating prevalence and substantial impact on global health (33). To date, resmetirom is the only pharmaceutical agent that has received approval from the US FDA for the treatment of MASLD (7). This compound exerts its therapeutic action by targeting the thyroid hormone receptor- β , which is the predominant isoform of the receptor in hepatocytes. Clinical studies have demonstrated that resmetirom effectively alleviates MASH, improves fibrosis, and reduces LDL

cholesterol levels. However, comparative analyses reveal that the use of resmetirom treatment is associated with a higher incidence of adverse effects, such as diarrhea and nausea, than placebo treatments (7). Additionally, concerns remain regarding the potential off-target effects of resmetirom on the thyroid hormone receptor- α (34), which could lead to cardiac and skeletal complications (35–37). Therefore, there is a pressing need for further studies to thoroughly assess the long-term safety profile and possible off-target effects of resmetirom.


Current research efforts are exploring alternative therapeutic strategies for MASLD. Clinical trial data suggest that therapies focusing on lipid metabolism regulation are more effective, while those targeting inflammation and fibrosis face challenges in altering the disease's progression (2, 5, 38). This is logic given that the primary pathophysiological mechanism in MASLD is the excess accumulation of TG in the liver, making treatments aimed at inflammation and fibrosis primarily palliative. Medications such as glucagon-like peptide-1 agonists, which are primarily used for weight reduction, have demonstrated significant therapeutic benefits for MASLD (39, 40). However, these therapies may not be appropriate for nonobese patients, who account for over 40% of all MASLD cases worldwide (41), highlighting the need of specialized interventions for patients with MASLD.

Our study, in concordance with previous findings, has observed the upregulation of *Plin2* in four commonly used MASLD/MASH models (14, 15), suggesting its potential as a therapeutic target. Despite its traditional role as a marker for LD (42), the development of PLIN2 inhibitor for MASLD therapy has been challenging due to the complexity of designing compounds that can directly interact with the PLIN2 protein. Recent advances in siRNA technology, including chemical modifications and the GalNAc-siRNA conjugate delivery system, have opened up new possibilities. These advancements have led to the development of innovative siRNA agents with improved stability, specificity, and transfection efficiency, while minimizing the activation of the innate immune system and reducing toxicity. Based on our findings and those of other studies, we propose that GalNAc-siPLIN2 could be

Scale bar, 50 μ m. C–E: Levels of hepatic TG (C), serum ALT (D), and serum AST (E) in humanized *PLIN2* knockin mice with HFD/HFr diet-induced MASH, following subcutaneous injection of 4 mg/kg GalNAc-si*Plin2*, GalNAc-siNC, or PBS. F: RT-qPCR analysis of relative mRNA levels of inflammation-related genes in liver tissues from humanized *PLIN2* knockin mice with HFD/HFr diet-induced MASH, following subcutaneous injection of 4 mg/kg GalNAc-si*Plin2*, GalNAc-siNC, or PBS. G: Hydroxyproline levels in liver tissues from humanized *PLIN2* knockin mice with HFD/HFr diet-induced MASH, following subcutaneous injection of 4 mg/kg GalNAc-si*Plin2*, GalNAc-siNC, or PBS. H: RT-qPCR analysis of relative mRNA levels of fibrosis-related genes were evaluated through RT-qPCR in liver tissues from humanized *PLIN2* knockin mice with HFD/HFr diet-induced MASH, following subcutaneous injection of 4 mg/kg GalNAc-si*Plin2*, GalNAc-siNC, or PBS. Data are shown as mean \pm SEM. For all panels, n = 6 mice per group. P values are determined using one-way ANOVA followed by Tukey's multiple comparison tests. "ns" denotes no significant difference. * $P < 0.05$, ** $P < 0.01$, and *** $P < 0.001$. ALT, alanine aminotransferase; AST, aspartate aminotransferase; GalNAc, N-acetylgalactosamine; IHC, immunohistochemistry; MASH, metabolic dysfunction-associated steatohepatitis; RT-qPCR, quantitative real-time PCR; TG, triglyceride.

a promising therapeutic option for MASLD, offering a potential treatment strategy for patients with diverse pathogenic mechanisms and the hope for improved clinical outcomes across a broad spectrum of MASLD patient populations.

Data availability

All data supporting this work will be available upon reasonable request from the corresponding author. 

Supplemental data

This article contains [supplemental data](#).

Acknowledgments

We are grateful to Drs Xiaowei Chen and Xiaoguang Lei for advice. We also thank Yating Hu, Yawei Wang, Maoxu Wang, and Jiashuo Wu for technical support, and Drs. Guilan Li, Yan Luo, Yonglu Tian and Jing Tian at the National Center for Protein Science at Peking University in Beijing, China, for the expertise in biochemical analysis, histology and behavioral experiments.

Author contributions

Y. W., M. L., and A. J. Z. writing–review and editing; Y. W., M. L., and A. J. Z. writing–original draft; Y. W. and J. Z. validation; Y. W., X. L., Y. Q., and Y. Z. methodology; Y. W. and Q. Y. data curation; Y. Z. and M. L. supervision; Y. Z., M. L., and A. J. Z. funding acquisition; A. J. Z. conceptualization.

Author ORCIDs

Yao Wang  <https://orcid.org/0000-0001-7008-691X>

Yifu Qiu  <https://orcid.org/0000-0001-5645-3189>

Yansong Zhang  <https://orcid.org/0000-0002-4996-8325>

Min Liu  <https://orcid.org/0000-0002-8077-0130>

Alan Jian Zhu  <https://orcid.org/0000-0001-8208-1729>

Funding and additional information

This work was supported by grants from the National Natural Science Foundation of China (32330026 to A. J. Z., and 32300990 to Y. Z.), National Key Research and Development Program of China (2019YFA0801500 to A. J. Z.), Peking University Chengdu Academy for Advanced Interdisciplinary Biotechnologies (to A. J. Z.), the Peking-Tsinghua Center for Life Sciences (to A. J. Z. and M. L.), the Ministry of Education Key Laboratory of Cell Proliferation and Differentiation (to A. J. Z.) and the China Postdoctoral Science Foundation (2023M730086 to Y. Z.). Y. W. was a Peking University President's Scholarship Awardee. Y. Z. was supported by a Peking University Boya Postdoctoral Fellowship.

Conflict of interest

A. J. Z., Y. W., M. L., Y. Z., and Q. Y. are named inventors of pending patent applications (2023106233979 to the Chinese Patent Office). The other authors declare that they have no conflicts of interest with the contents of this article.

Abbreviations

AAV, adeno-associated virus; ALT, alanine aminotransferase; AST, aspartate aminotransferase; BAT, brown

adipose tissue; FDA, Food and Drug Administration; gRNA, guide RNA; GalNAc, N-acetylgalactosamine; GTT, glucose tolerance; HFD, high-fat diet; HFr, high fructose; HYP, hydroxyproline; ITT, insulin tolerance test; KI, knockin; LD, lipid droplet; MASLD, metabolic dysfunction–associated steatotic liver disease; MASH, metabolic dysfunction-associated steatohepatitis; PBST, PBS plus 0.1% Tween-20; PEI, polyethylenimine; PFA, paraformaldehyde; RT-qPCR, quantitative real-time PCR; sgRNA, small guide RNA; TC, total cholesterol; TG, triglyceride.

Manuscript received April 27, 2024, and in revised form July 10, 2024. Published, JLR Papers in Press, August 24, 2024, <https://doi.org/10.1016/j.jlr.2024.100635>

REFERENCES

1. Le, M. H., Le, D. M., Baez, T. C., Wu, Y., Ito, T., Lee, E. Y., *et al.* (2023) Global incidence of non-alcoholic fatty liver disease: a systematic review and meta-analysis of 63 studies and 1,201,807 persons. *J. Hepatol.* **79**, 287–295
2. Friedman, S. L., Neuschwander-Tetri, B. A., Rinella, M., and Sanyal, A. J. (2018) Mechanisms of NAFLD development and therapeutic strategies. *Nat. Med.* **24**, 908–922
3. Wong, V. W., Ekstedt, M., Wong, G. L., and Hagström, H. (2023) Changing epidemiology, global trends and implications for outcomes of NAFLD. *J. Hepatol.* **79**, 842–852
4. Huang, D. Q., Mathurin, P., Cortez-Pinto, H., and Loomba, R. (2023) Global epidemiology of alcohol-associated cirrhosis and HCC: trends, projections and risk factors. *Nat. Rev. Gastroenterol. Hepatol.* **20**, 37–49
5. Harrison, S. A., Allen, A. M., Dubourg, J., Noureddin, M., and Alkhoufi, N. (2023) Challenges and opportunities in NASH drug development. *Nat. Med.* **29**, 562–573
6. Powell, E. E., Wong, V. W., and Rinella, M. (2021) Non-alcoholic fatty liver disease. *Lancet.* **397**, 2212–2224
7. Harrison, S. A., Bedossa, P., Guy, C. D., Schattenberg, J. M., Loomba, R., Taub, R., *et al.* (2024) A phase 3, randomized, controlled trial of resmetirom in NASH with liver fibrosis. *N. Engl. J. Med.* **390**, 497–509
8. Cai, H., Qin, Y. L., Shi, Z. Y., Chen, J. H., Zeng, M. J., Zhou, W., *et al.* (2019) Effects of alternate-day fasting on body weight and dyslipidaemia in patients with non-alcoholic fatty liver disease: a randomised controlled trial. *BMC Gastroenterol.* **19**, 219
9. Varady, K. A., Cienfuegos, P., Ezpeleta, M., and Gabel, K. (2022) Clinical application of intermittent fasting for weight loss: progress and future directions. *Nat. Rev. Endocrinol.* **18**, 309–321
10. Goh, V. J., and Silver, D. L. (2013) The lipid droplet as a potential therapeutic target in NAFLD. *Semin. Liver Dis.* **33**, 312–320
11. Scorletti, E., and Carr, R. M. (2022) A new perspective on NAFLD: focusing on lipid droplets. *J. Hepatol.* **76**, 934–945
12. Bickel, P. E., Tansey, J. T., and Welte, M. A. (2009) PAT proteins, an ancient family of lipid droplet proteins that regulate cellular lipid stores. *Biochim. Biophys. Acta.* **1791**, 419–440
13. Listenberger, L. L., Ostermeyer-Fay, A. G., Goldberg, E. B., Brown, W. J., and Brown, D. A. (2007) Adipocyte differentiation-related protein reduces the lipid droplet association of adipose triglyceride lipase and slows triacylglycerol turnover. *J. Lipid Res.* **48**, 2751–2761
14. Motomura, W., Inoue, M., Ohtake, T., Takahashi, N., Nagamine, M., Tanno, S., *et al.* (2006) Up-regulation of ADRP in fatty liver in human and liver steatosis in mice fed with high fat diet. *Biochem. Biophys. Res. Commun.* **340**, 1111–1118
15. Zhao, W., Zhang, Y., Lin, S., Li, Y., Zhu, A. J., Shi, H., *et al.* (2023) Identification of Ubr1 as an amino acid sensor of steatosis in liver and muscle. *J. Cachexia Sarcopenia Muscle.* **14**, 1454–1467
16. Chang, B. H., Li, L., Paul, A., Taniguchi, S., Nannegari, V., Heird, W. C., *et al.* (2006) Protection against fatty liver but normal adipogenesis in mice lacking adipose differentiation-related protein. *Mol. Cell Biol.* **26**, 1063–1076
17. Libby, A. E., Bales, E., Orlicky, D. J., and McManaman, J. L. (2016) Perilipin-2 deletion impairs hepatic lipid accumulation by

- interfering with sterol regulatory element-binding protein (SREBP) activation and altering the hepatic lipidome. *J. Biol. Chem.* **291**, 24231–24246
18. Zhang, Y., Lin, S., Peng, J., Liang, X., Yang, Q., Bai, X., *et al.* (2022) Amelioration of hepatic steatosis by dietary essential amino acid-induced ubiquitination. *Mol. Cell.* **82**, 1528–1542
 19. Jumper, J., Evans, R., Pritzel, A., Green, T., Figurnov, M., Ronneberger, O., *et al.* (2021) Highly accurate protein structure prediction with AlphaFold. *Nature.* **596**, 583–589
 20. Croke, S. T., Witztum, J. L., Bennett, C. F., and Baker, B. F. (2018) RNA-targeted therapeutics. *Cell Metab.* **27**, 714–739
 21. Huang, Y., Zheng, S., Guo, Z., de Mollerat du Jeu, X., Liang, X. J., Yang, Z., *et al.* (2022) Ionizable liposomal siRNA therapeutics enables potent and persistent treatment of Hepatitis B. *Signal. Transduct. Target. Ther.* **7**, 38
 22. Platt, R. J., Chen, S., Zhou, Y., Yim, M. J., Swiech, L., Kempton, H. R., *et al.* (2014) CRISPR-Cas9 knockin mice for genome editing and cancer modeling. *Cell.* **159**, 440–455
 23. Wang, X., Wang, H., Xu, B., Huang, D., Nie, C., Pu, L., *et al.* (2021) Receptor-mediated ER export of lipoproteins controls lipid homeostasis in mice and humans. *Cell Metab.* **33**, 350–366
 24. Loomba, R., Friedman, S. L., and Shulman, G. I. (2021) Mechanisms and disease consequences of nonalcoholic fatty liver disease. *Cell.* **184**, 2537–2564
 25. Hu, B., Zhong, L., Weng, Y., Peng, L., Huang, Y., Zhao, Y., *et al.* (2020) Therapeutic siRNA: state of the art. *Signal. Transduct. Target. Ther.* **5**, 101
 26. Weng, Y., Xiao, H., Zhang, J., Liang, X. J., and Huang, Y. (2019) RNAi therapeutic and its innovative biotechnological evolution. *Biotechnol. Adv.* **37**, 801–825
 27. Springer, A. D., and Dowdy, S. F. (2018) GalNAc-siRNA conjugates: leading the way for delivery of RNAi therapeutics. *Nucleic Acid Ther.* **28**, 109–118
 28. Robbins, M., Judge, A., and MacLachlan, I. (2009) siRNA and innate immunity. *Oligonucleotides.* **19**, 89–102
 29. Liu, Z., Zhang, Y., Graham, S., Wang, X., Cai, D., Huang, M., *et al.* (2020) Causal relationships between NAFLD, T2D and obesity have implications for disease subphenotyping. *J. Hepatol.* **73**, 263–276
 30. Choi, S. E., Hwang, Y., Lee, S. J., Jung, H., Shin, T. H., Son, Y., *et al.* (2022) Mitochondrial protease ClpP supplementation ameliorates diet-induced NASH in mice. *J. Hepatol.* **77**, 735–747
 31. Gurtner, G. C., Werner, S., Barrandon, Y., and Longaker, M. T. (2008) Wound repair and regeneration. *Nature.* **453**, 314–321
 32. Schwabe, R. F., Tabas, I., and Pajvani, U. B. (2020) Mechanisms of fibrosis development in nonalcoholic steatohepatitis. *Gastroenterology.* **158**, 1913–1928
 33. Adams, L. A., Roberts, S. K., Strasser, S. I., Mahady, S. E., Powell, E., Estes, C., *et al.* (2020) Nonalcoholic fatty liver disease burden: Australia, 2019-2030. *J. Gastroenterol. Hepatol.* **35**, 1628–1635
 34. Kelly, M. J., Pietranico-Cole, S., Larigan, J. D., Haynes, N. E., Reynolds, C. H., Scott, N., *et al.* (2014) Discovery of 2-[3,5-dichloro-4-(5-isopropyl-6-oxo-1,6-dihydropyridazin-3-yloxy)phenyl]-3,5-dioxo-2,3,4,5-tetrahydro[1,2,4]triazine-6-carbonitrile (MGL-3196), a Highly Selective Thyroid Hormone Receptor β agonist in clinical trials for the treatment of dyslipidemia. *J. Med. Chem.* **57**, 3912–3923
 35. Bassett, J. H., and Williams, G. R. (2003) The molecular actions of thyroid hormone in bone. *Trends Endocrinol. Metab.* **14**, 356–364
 36. Simonides, W. S., Thelen, M. H., van der Linden, C. G., Muller, A., and van Hardeveld, C. (2001) Mechanism of thyroid-hormone regulated expression of the SERCA genes in skeletal muscle: implications for thermogenesis. *Biosci. Rep.* **21**, 139–154
 37. Klein, I., and Danzi, S. (2016) Thyroid disease and the heart. *Curr. Probl. Cardiol.* **41**, 65–92
 38. Vuppalanchi, R., Noureddin, M., Alkhoury, N., and Sanyal, A. J. (2021) Therapeutic pipeline in nonalcoholic steatohepatitis. *Nat. Rev. Gastroenterol. Hepatol.* **18**, 373–392
 39. Patel Chavez, C., Cusi, K., and Kadiyala, S. (2022) The emerging role of glucagon-like peptide-1 receptor agonists for the management of NAFLD. *J. Clin. Endocrinol. Metab.* **107**, 29–38
 40. Jastreboff, A. M., Kaplan, L. M., Frias, J. P., Wu, Q., Du, Y., Gurbuz, S., *et al.* (2023) Triple-hormone-receptor agonist retatrutide for obesity - a phase 2 trial. *N. Engl. J. Med.* **389**, 514–526
 41. Ye, Q., Zou, B., Yeo, Y. H., Li, J., Huang, D. Q., Wu, Y., *et al.* (2020) Global prevalence, incidence, and outcomes of non-obese or lean non-alcoholic fatty liver disease: a systematic review and meta-analysis. *Lancet Gastroenterol. Hepatol.* **5**, 739–752
 42. Pillai, S., Mahmud, I., Mahar, R., Griffith, C., Langsen, M., Nguyen, J., *et al.* (2022) Lipogenesis mediated by OGR1 regulates metabolic adaptation to acid stress in cancer cells via autophagy. *Cell Rep.* **39**, 110796